Mechanically Assisted Neurorehabilitation: A Novel Six-Bar Linkage Mechanism for Gait Rehabilitation

Mi Li, Jianqiang Yan, Haiming Zhao, Guozhi Ma, and Yihang Li

***Abstract*— Repeated and intensive gait training can improve muscle strength and movement coordination of patients with neurological or orthopedic impairments. However, conventional physical therapy by a physiotherapist is laborious and expensive. Therefore, this therapy is not accessible for the majority of patients. This paper presents a six-bar linkage mechanism for human gait rehabilitation with a natural ankle trajectory. Firstly, a six-bar linkage mechanism is selected as the original mechanism to construct a gait rehabilitation device. Then the ankle trajectory is formulated as a function of the crank angle. And the rotation angle of the crank is set as a linear function of time. Therefore, constant speed motor is sufficient to control the mechanism. For the dimensional synthesis, the precise point distances of the gait trajectory and the coupler curve are set as objective functions, with the kinematic constraints including in the optimization procedure. To obtain the optimal structure design parameters, a cooperative dual particle swarm optimization algorithm is developed. The results show that the coupler curve matches well with the gait trajectory. The average distance between the 60 precision points is 3.5 mm.**

***Index Terms*— Stroke, gait rehabilitation, six-bar linkage mechanism, end-effector, dual particle swarm optimization.**

I. Introduction

STROKE is one of the leading causes of permanent disability worldwide, with nearly two thirds of the survivors suffering from paralysis or hemiplegia, and experiencing problems with daily activities such as walking [1], [2]. Research results have shown that the human brain is capable of self-reorganization, or neuroplasticity. And physical therapy offers an opportunity for exercise recovery [3], [4]. We observed that physical therapy can help people improve their basic activities of daily living after stroke [5], [6]. However, the fact that conventional physical therapy is laborious and expensive makes these therapies less adequate for home healthcare. Therefore, the rehabilitation robot system is a good choice for physical therapy [7]. Over the last decades, several lower limb rehabilitation robots have been developed to restore mobility of the affected limbs [8]. These systems can be simply classified into five types according to the structure [8]: (i) treadmill gait trainers, e. g. LokoHelp, ALEX, Ramanpreet [9]–[11] (ii) foot plate-based gait trainers, e. g. Yoon, J [12], [13] (iii) overground gait trainers, e. g. KineAssist, WalkTrainer [14], [15] (iv) stationary gait trainers, e. g. Palestra, Lambda, Mohan [16]–[18] and (v) ankle rehabilitation systems, e. g. Rutgers Ankle, AKROD [19], [20]. However, some of these rehabilitation robots are large and costly. It's usually only used in large medical centers. Other small rehabilitation robots proposed by the researchers need further improvement.

In the rehabilitation robot system, end-effector gait trainers have attracted the attention of researchers [21], [22]. Several trials have been published on the efficacy of end-effector gait trainers [23]–[26]. The results of Bevilacqua's study showed that the end-effector gait trainer is effective for subacute stroke patients with a lower function ambulation assessment, showing significant changes in independent walking ability [27]. The end-effector gait trainer is mainly composed of gait simulation mechanism, ankle joint posture guidance mechanism and gravity support system [28]. During the exercises, the trainee stands on the pedal at the end of the mechanism with the help of the therapist, and the trainee's feet are driven to complete the walking training action through the pedal. Since the end-effector gait trainer does not impose constraints on the trainee's knee joint, the therapist can correct the movement of the trainee's knee joint as needed [29]. So that the rehabilitation treatment can achieve better results [22]. At the same time, the end effector gait trainer can also use functional electrical stimulation during the exercise [28].

To simulate gait, several linkage mechanism or cam linkage mechanism have been proposed, such as the four-bar linkage mechanism proposed by Alves [30], the Stephenson II/III six-bar mechanism proposed by Wang and Tsuge [31], [32], the ten-bar linkage mechanism presented by McCarthy [33], the cam linkage mechanism established by Gonçalves and Smith [34], [35], the cam gear mechanism established by Soong [36]. However, all the mechanism proposed in these literatures must be controlled using servomotors. Thus,

Manuscript received October 12, 2020; revised February 11, 2021 and March 28, 2021; accepted May 16, 2021. Date of publication May 19, 2021; date of current version June 7, 2021. This work was supported in part by the National Natural Science Foundation of China under Grant 51801062 and in part by the College Students' Innovative Experimental Project under Grant 2019126. *(Corresponding author: Jianqiang Yan.)*

This work involved human subjects or animals in its research. Approval of all ethical and experimental procedures and protocols was granted by the Biomedical Research Ethics Committee of Hunan Normal University under Approval No. 2020056.

Mi Li, Jianqiang Yan, Guozhi Ma, and Yihang Li are with the School of Engineering and Design, Hunan Normal University, Changsha 410081, China (e-mail: 475431371@qq.com).

Haiming Zhao is with the School of Mechanical and Electrical Engineering, Central South University, Changsha 410083, China.

Digital Object Identifier 10.1109/TNSRE.2021.3081706

Shao [37] established a cam linkage mechanism. In their research, the time sequence of the required trajectories was considered, so only a constant speed motor was needed to control the mechanism. However, a cam is needed to correct the errors.

For the dimensional synthesis, Yuan [38] presented a method to modify the output motion of a linkage mechanism. Bhatia and Bagci [39] proposed an optimization method for path synthesis of six-bar linkage mechanism. Mehdigholi [40] presented a method to optimization of watt's six-bar linkage mechanism and used genetic algorithm for global search. Ma [41] used the optimization theory to complete the dimensional synthesis of spiral drum screen. As Nollexa [42] indicated that linkage mechanism design equations have many local optima, how to find the global minimum is key factor to achieve the dimensional synthesis. The Particle Swarm Optimization (PSO) algorithm and genetic algorithm have been applied successfully in dimensional synthesis for mechanism [43], [44]. The traditional genetic algorithm [45] can increase the probability of finding the global minimum by increasing the population size. However, the increase in population size will make the convergence speed of genetic algorithm decrease rapidly or fail to converge. Other algorithms for solving linear programming or nonlinear convex optimization problems, such as the interior point method, tend to be trapped in local optima in the solution of linkage design equations [46]. For the PSO algorithm, the researchers have made some beneficial improvements [47]–[50]. Among them, the improved scheme using multiple groups of particles has attracted researcher's attention [51]–[55]. Zheng proposed a Cooperative Dual-swarm PSO algorithm to improve the ability of PSO in deal with dynamic optimization problems [51]. Hu proposed an endocrine cooperative particle swarm optimization algorithm for routing recovery problem. In the iterative process, the mutation direction of the particle is determined by multi-swarm evolution equation [52]. Mohammed proposed a discrete cooperative particle swarm optimization algorithm for the routing of integrated circuits. Although two groups of particles are used to search, there is no information interaction between them [53]. He used damping factor and cooperation mechanism to improve the performance of particle swarm optimization algorithm [54]. Hajer proposed a modified scheme that uses two groups of particles to search. In their research, the first one performs exploration while the second one is responsible for exploitation [55]. This is beneficial to restrain the premature convergence of the algorithm. These previous works provided a good foundation for finding the global minimum of linkage mechanism design equations.

The purpose of this paper is to provide a gait rehabilitation system for home healthcare with low cost. A new link mechanism for generating accurate gait trajectories is proposed. The design and optimization methods are also presented. In the dimensional optimization, the time sequence of the trajectory is considered in order to obtain the required trajectory at a constant input speed. To obtain the optimal structure design parameters, a Cooperative Dual Particle Swarm Optimization algorithm (CDPSO) is developed. The results show that this linkage can make its coupler curve through 60 precision points.

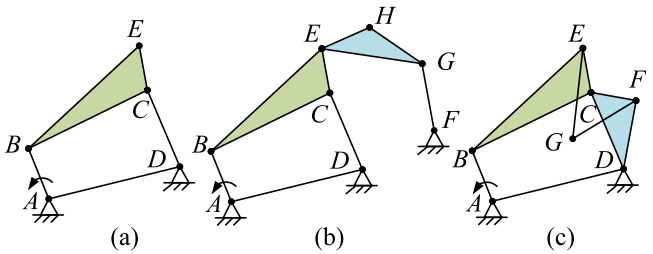

Fig. 1. Sketches of gait trajectory generation. (a) four-bar linkage mechanism. (b) Stephenson III six-bar linkage mechanism. (c) six-bar linkage mechanism.

The novelties and contributions of this paper are listed as follows.

1) A six-bar linkage mechanism is proposed to produce accurate gait trajectories, thereby avoiding the production of complex cams. It is beneficial to further reduce the cost of the gait generation mechanism.

2) The time sequence of the required trajectories is considered, only a constant speed motor is needed to control the mechanism.

3) The optimal design parameters of the structure proposed in this paper can be achieved by applying the CDPSO algorithm.

II. Conceptual Design

Kapovich [56] pointed out that any plane algebraic curve has an associated linkage which can trace the curve. Therefore, the single degree of freedom linkage system is used to track the gait trajectory. Alves [30] proposed a four-bar linkage mechanism (Fig. 1(a)) for gait trajectory generation. However, the four-bar linkage mechanism can only track 5 points accurately, which makes the generated trajectory deviate from the natural gait trajectory. The six-bar linkage mechanism has two more bars than the four-bar linkage mechanism, making it able to track more points. Dordevic [57] used a gradient optimizer to the design a Stephenson III six-bar linkage mechanism (Fig. 1(b)) which fits 32 specified points on the trajectory. However, a servomotor must be used to control the rotation of the crank. On the other hand, since another four-bar linkage mechanism is connected in series with the four-bar linkage mechanism proposed by Alves [30], more space is required. Thus, we propose a new six-bar linkage mechanism for gait path generation (Fig. 1(c)). The coupler curve of the six-bar linkage mechanism is expected to pass through all precision points on the gait trajectory, which are defined by two independent x and y coordinates. In addition, it is desirable to be able to use a constant speed motor to control the trajectory generating device, thereby avoiding the use of complex control systems. For this purpose, we will investigate the dimensional synthesis of the mechanism in the following section.

III. Dimensional Synthesis

A. Lower Limb Kinematics Model

To obtain the required gait trajectory, Onen [49] developed a simple lower limb kinematics model based on the clinical

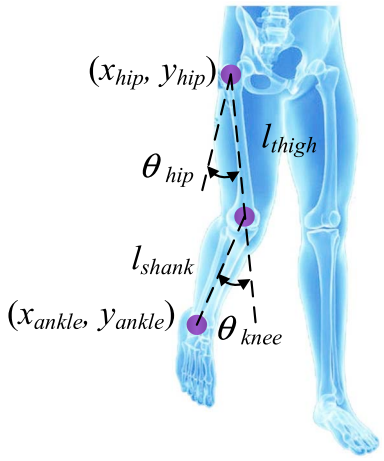

Fig. 2. Human lower limb model.

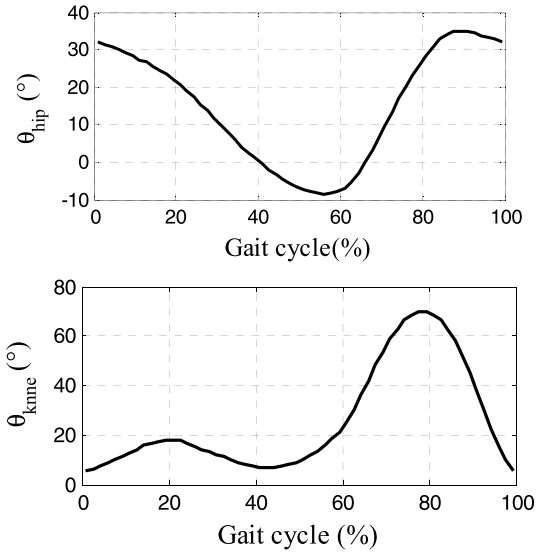

Fig. 3. Hip and knee angle.

gait analysis specification gait database.

$$x_{ankle} = -l_{thigh}\sin\theta_{hip} + l_{shank}\sin(\theta_{knee} - \theta_{hip}) + x_{hip}$$
$$y_{ankle} = -l_{thigh}\cos\theta_{hip} - l_{shank}\cos(\theta_{knee} - \theta_{hip}) + y_{hip} \quad (1)$$

As shown in Fig. 2, where (x_{ankle}, y_{ankle}) is the Cartesian coordinates of ankle joint, (x_{hip}, y_{hip}) is the Cartesian coordinates of hip joint, $(\theta_{hip}, \theta_{knee})$ are the hip and knee angles, (l_{thigh}, l_{shank}) are the lengths of the thigh and shank. As Pedro Alves [30] pointed out, it can be calculated based on the height of the subject (hg), $l_{thigh} = 0.235\ hg$), $l_{shank} = 0.228\ hg$).

The hip and knee angles of a normal gait are shown in Fig. 3, which is obtained through a human gait capture experiment. The subject of the gait capture experiment is a healthy adult woman, whose height is 1630mm, weight is 52kg. And the length of the thigh and shank are 383mm and 372mm, respectively. The spatial coordinate information of the marker points placed on the limb of the subject is captured by an infrared camera unit arranged on the side of the treadmill. The sampling frequency of the spatial coordinate acquisition system is 100 Hz, and the resolution is 0.1mm. The gait cycle curves of the hip and knee angle are obtained through the movement analysis of the collected spatial coordinate

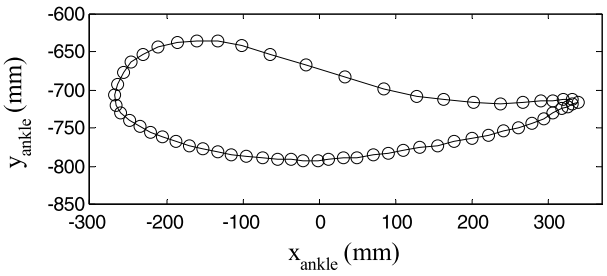

Fig. 4. Gait trajectory.

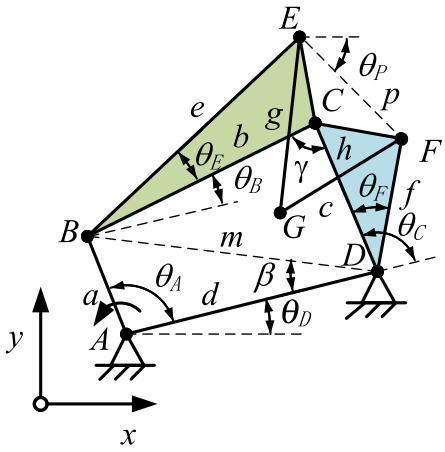

Fig. 5. Geometric parameters of the six-bar linkage mechanism.

information of the marker points. Sample the hip and knee angles based on constant time intervals. Then input them into the lower limb kinematics model written as equation (1). The gait trajectory of the subject with the hip joint fixed in the vertical direction can be obtained. As shown in Fig. 4, it is a gait trajectory of a subject with a height of 1630 mm. In Fig. 4, the hollow circles are precision points on the trajectory, which are obtained by sampling the hip and knee angles at equal intervals. The number of sampling points is 60.

B. Kinematic Analysis

The selected six-bar mechanism for developing this project is shown in Fig. 5. As shown in Fig. 5, a, b, c, d, e, f, g, h are the lengths of each link. The angles of each link a, b and c relative to link d are θ_A, θ_B, θ_C. The Angle between link d and the x-axis is θ_D. θ_E, θ_F are structural angles. x_A, y_A are the Cartesian coordinates of point A. γ is the transmission angle.

The Cartesian coordinates of the point E on the plane of the link b can be obtained:

$$x_E = x_A + a * cos(\theta_A + \theta_D) + e * cos(\theta_B + \theta_E + \theta_D)$$
$$y_E = y_A + a * sin(\theta_A + \theta_D) + e * sin(\theta_B + \theta_E + \theta_D) \quad (2)$$

where,

$$\theta_B = arccos\frac{b^2 + m^2 - c^2}{2bm} - \beta \quad (3)$$
$$\beta = arcsin\frac{a * sin\theta_A}{m} \quad (4)$$
$$m = \sqrt{a^2 + d^2 - 2ad * cos\theta_A} \quad (5)$$

Similarly, the Cartesian coordinates of the point F on the plane of the connecting link c can be obtained as:

$$\begin{aligned} x_F &= x_A + d * cos\theta_D + f * cos(\theta_C + \theta_D - \theta_F) \\ y_F &= y_A + d * sin\theta_D + f * sin(\theta_C + \theta_D - \theta_F) \end{aligned} \tag{6}$$

where,

$$\theta_C = \pi - arccos\frac{c^2 + m^2 - b^2}{2mc} - \beta \tag{7}$$

Combining the coordinates of points E, F and the lengths of the links g, h, we can get the coordinates of point G as:

$$\begin{aligned} x_G &= x_E + g * cos(\theta_P - \text{arccos}(\frac{g^2 + p^2 - h^2}{2gp})) \\ y_G &= y_E + g * sin(\theta_P - \text{arccos}(\frac{g^2 + p^2 - h^2}{2gp})) \end{aligned} \tag{8}$$

where p is the distance between points E and F.

$$p = \sqrt{(x_F - x_E)^2 + (y_F - y_E)^2} \tag{9}$$

$$\theta_P = \begin{cases} arctan\left(\dfrac{y_F - y_E}{x_F - x_E}\right) & \theta_G \epsilon [-\dfrac{\pi}{2}, \dfrac{\pi}{2}] \\ arctan\left(\dfrac{y_F - y_E}{x_F - x_E}\right) + \pi & \theta_G \epsilon (\dfrac{\pi}{2}, \dfrac{3\pi}{2}] \end{cases} \tag{10}$$

IV. Optimization

A. The Range of the Design Parameters

Refer to (8), the coordinates of the point G are determined by 14 independent variables such as the lengths of each link and the initial rotation angle θ_i of the crank a. Therefore, the design vector of the six-bar linkage mechanism can be described as:

$$X = [a, b, c, d, e, \theta_E, x_A, y_A, \theta_D, f, \theta_F, g, h, \theta_i]^T \tag{11}$$

B. Objective Function

This paper aims to design a six-bar linkage mechanism for generating natural gait trajectory. In this mechanism, only a constant speed motor is needed to control the rotation of the crank to meet the natural gait phase. Therefore, the rotation angle of the crank is equally divided into n equal parts, where n is the number of precision points on the target trajectory. Then, the distance between the point G on the six-bar linkage mechanism and each precise point on the target trajectory can be set as the objective function.

$$minf\,(X) = min\sum_{i=1}^{n}\sqrt{\left(x_G^{(i)} - x_{ankle}^{(i)}\right)^2 + \left(y_G^{(i)} - y_{ankle}^{(i)}\right)^2} \tag{12}$$

where n is the number of precision points on the target trajectory, which is given as 60 in this paper.

C. Constraints

1) The Grashof Criterion: In order to ensure that the crank can rotate freely, the sum of the lengths of the longest and shortest links in the four-bar linkage mechanism should be less than the sum of the lengths of the other two links. When the links between a and b are collinear twice, the condition of the existence of the crank can be obtained from the relationship of the side length of the triangle. Therefore, the Grashof criterion constraint can be given as follows:

$$\begin{cases} g_1\,(X) = a + d - b - c \le 0 \\ g_2\,(X) = a + b - c - d \le 0 \\ g_3\,(X) = a + c - b - d \le 0 \end{cases} \tag{13}$$

2) Minimum Transmission Angle: In order to obtain better force transmission performance, the minimum transmission angle of the mechanism should be greater than the allowable transmission angle γ_0. For a crank-rocker mechanism, the minimum transmission angle appears at one of two positions where the crank a and the frame d are collinear. The constraint is given by:

$$\begin{cases} g_4\,(X) = b^2 + c^2 - (d - a)^2 - 2bc * cos\gamma_0 \le 0 \\ g_5\,(X) = b^2 + c^2 - (d + a)^2 - 2bc * cos\gamma_0 \le 0 \end{cases} \tag{14}$$

where γ_0 is the allowable transmission angle, which is given as $\pi/6$ in this paper.

3) Assembly Conditions: When $p > g + h$ or $p < |g\text{-}h|$, links g and h cannot be assembled. Thus, the constraints are:

$$\begin{cases} g_6\,(X) = -g - h + p \le 0 \\ g_7\,(X) = g - h - p \le 0 \\ g_8\,(X) = -g + h - p \le 0 \end{cases} \tag{15}$$

where, p is the distance between points E and F.

In order to realize the optimization algorithm, the multiconstrained optimization problem is transformed into an unconstrained optimization problem by using the penalty function method. A new objective function is constructed as follows:

$$\Phi\left(X, r^{(k)}\right) = f\,(X) + r^{(k)}\sum_{u=1}^{8} max\,[0, g_u\,(X)]^2 \tag{16}$$

where, $g_u\,(X)$ is the inequality constraint; and $r^{(k)}$ is the penalty factor. We set $r^{(k)}$ as a positive increasing sequence $0 < r^{(1)} < r^{(2)} \cdots < r^{(k)}$. When a constraint is violated, a large value penalty factor $r^{(k)}$ is multiplied to the inequality constraint $g_u\,(X)$. The variable k is the count of times the constraint condition is not met. Thus, the infeasible solutions have much larger cost functions than the feasible ones.

D. Cooperative Double Particle Swarm Optimization Algorithm

As Nollexa [42] indicated that linkage design equations have many local optima. How to find the global minimum is another key factor to achieve the dimensional synthesis of the linkage mechanism.

Therefore, a CDPSO algorithm is developed to synthesize the size of the linkage mechanism. The PSO algorithm proposed by Eberhart [59] is shown in (17) and (18).

$$v_i(k+1) = \omega v_i(k) + c_1 rand()(pbest_i - x_i(k)) + c_2 rand()(gbest - x_i(k)) \quad (17)$$

$$x_i(k+1) = x_i(k) + v_i(k+1) \quad (18)$$

where i is the number of particles, $v_i(k)$ is the ith particle's velocity in the kth iteration, $x_i(k)$ is the position of the ith particle in the kth iteration, p_{best} is the historical personal best position, g_{best} is the historical global best position, ω is the inertial weight, c_1 and c_2 are positive accelerating constants, *rand* () is a random function with the range [0,1].

Eberhart [59] pointed out that larger inertia weight can improve the global search capability of the PSO algorithm. A relatively small inertia weight is more conducive to the local search of the PSO algorithm. Therefore, the CDPSO algorithm strategy is to use two groups of particles with different inertia weights to search at the same time. The optimal location information and search space are exchanged during the search process. Selecting appropriate inertia weights for the two groups of particles makes the first group of particles mainly used for global search, and the second group of particles mainly used for accurately search. If the optimal solution of the first group is better than the second group, the search positions and search spaces of the two particles are exchanged. The two groups of particles that exchange search positions and search spaces continue to search until the final conditions are met. In the iteration process, if the best positions of the two groups of particles are at the edge of the feasible region, expand the side of the feasible region and reduce the other side. By exchanging the best position and search spaces of the two groups of particles continuously, it is possible to avoid premature convergence of the iteration and improve the search accuracy of the algorithm.

Since a larger inertia weight can improve the global search ability, the inertia weight update strategy of the first group can be set to the following equation.

$$\omega_1 = \omega_{\max} - (\omega_{\max} - \omega_{\min}) \frac{k^2}{T^2} \quad (19)$$

where, ω_1 denotes the inertial weight in the first group; $\omega_{\max}$ and $\omega_{\min}$ are the maximum and minimum values of the inertial weight; k is the current iteration number; T is the maximum iteration. In (19), the inertia weight is a quadratic function of iteration number. The inertia weights change slowly during the initial iteration, which is useful for global search. Near the maximum number of iterations, the inertia weights vary similarly to the linear decreasing strategy, which is conducive to convergence to the global optimum.

The second group is designed for accurate search. Thus, the inertia weight of the second group is described as equation (20).

$$\omega_2 = \omega_{\min} + (\omega_{\max} - \omega_{\min}) \left[1 - logsig(\frac{\alpha k}{T} - \beta) \right] \quad (20)$$

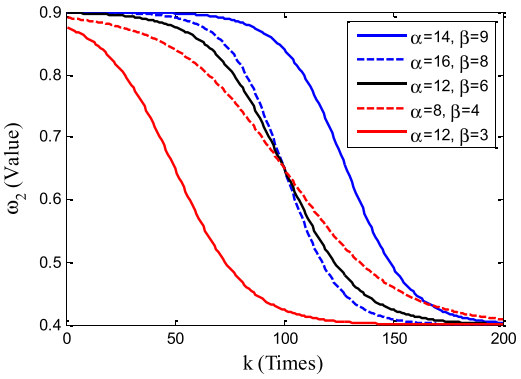

Fig. 6. Variations of inertia weights with iterations for different α and β.

where ω_2 denote the inertial weight in the second group. *logsig*( ) is sigmoid function. α and β are the feature parameters.

The variations of inertia weights with iterations for different α and β is shown in the Fig.6. Where, $\omega_{\max} = 0.9$, $\omega_{\min} = 0.4$, T = 200.

From the Fig.6, we know that the values of α and β determine the changing trend of the inertia weights. When α and β are set to larger values, the inertia weight can decrease at a slower speed in the beginning and the end. When the values of α and β are small, the decreasing speed of the inertial weight will increase. When α is twice as much as β, the inertia weight is centrosymmetric. Based on the above analysis, we set $\alpha = 12$ and $\beta = 6$.

The steps of the CDPSO algorithm applied to the optimal value search of the objective function are as follows:

Step 1. Set the initial population number, initial velocity, position of the two groups of particles. Set the allowed iterations, and accuracy.

Step 2. For each group, calculate the objective function value according to (16), save the historical personal best position, historical global best position.

Step 3. Calculate the inertia weights of the two groups of particles according to (19) and (20).

Step 4. Update the positions and velocities of the two groups of particles according to (17) and (18).

Step 5. Recalculate the particle objective function value according to the updated particle position, and update the historical personal best position, historical global best position.

Step 6. Compare the group's best objective function value of the two groups. If the first group's best objective function value better than that of the second group, the position and inertia weight of the two groups are exchanged.

Step 7. If the termination condition is met, stop the search, and output the optimization result, otherwise go to step 2. The termination condition is that the number of iterations exceeds allowed iterations or the reduction of the objective function is less than the allowed accuracy.

To test the performance of the CDPSO algorithm, two typical test functions are used for testing and compared with linearly decreasing weight particle swarm optimization algorithm (LDWPSO). The two test functions are described in

TABLE I
THE COMPARATIVE RESULTS OF TWO ALGORITHMS

Function	CDPSO		LDWPSO	
	N	F	N	F
f_1	0	1.0054	6	0.9959
f_2	20	6.1	54	11.26

the following equations [54].

$$\max f_1 = \frac{\sin\sqrt{x^2+y^2}}{\sqrt{x^2+y^2}} + \exp\left(\frac{\cos 2\pi x + \cos 2\pi y}{2}\right) - \mathrm{e}, \quad |x, y| \le 10$$

$$\min f_2 = \sum_{i=1}^{10}\left[x_i^2 - 10\cos(2\pi x_i) + 10\right], \quad |x_i| \le 5.12 \quad (21)$$

According to Liang's research results [60], we set the particle speed range of the two algorithms as [0.1, 1], the population size as 50, the acceleration factors c_1 and c_2 as 1.49445, the maximum and minimum inertia weights as 0.9 and 0.4, respectively, and the number of iterations as 1,000. In 100 optimization calculations, the number of times N and the average optimal function value F are shown in Table I. N is the algorithm falls into the local optimal solution (the absolute error between the optimization result and the global optimal value is greater than 10^{-4} is regarded as the local optimal solution).

It can be seen from Table I that the CDPSO algorithm proposed in this paper can effectively prevent the algorithm from falling into the local optima and improve the reliability and accuracy of the optimization result.

V. NUMERICAL IMPLEMENTATION

The numerical implementations of two subjects with different heights are presented in this section. And the proposed method is applied to synthesize a six-bar linkage mechanism as shown in Fig.5.

In the first case, the height of the subject is 1630 mm, whose gait trajectory is shown in Fig.4. The proposed algorithm is applied to search for optimal design parameters. The parameters of the algorithm are set as follows. The population sizes of both groups of particles are 100, and the maximum iteration number is 500.

In order to limit the size of the link and make the whole mechanism with an appropriate size, the boundary of each link, as shown in Table II.

According to the design parameters boundaries shown in Table II, the optimal design parameters of the six-bar linkage mechanism are obtained, which are shown in Table III. It can be found that the length of each link is less than 550 mm. The longest link is b, which is 548 mm. The maximum link length of the mechanism proposed in [37] is 771 mm. The data in this article illustrates our advantages.

According to the optimal design parameters shown in Table III, the coupler curve is generated as shown in Fig.7 (a) by driving the crank at a constant speed. From Fig.7 (a), it can be found that the coupler curve matches well with the gait trajectory. The average distance between the 60 precision points is 3.5 mm. The maximum distance is 12 mm, and the sum of distances is 225 mm. It has similar accuracy, compared with the results presented in [37]. But it is not necessary to use a cam or a servomotor as mentioned in [37]. The final sketch of the six-bar linkage mechanism is shown in Fig.8 (a).

Furthermore, to illustrate the applicability of the proposed method, the second case is presented in this section. In this case, the height of the subject is 1800 mm. Based on the same design parameter boundaries, the optimal design parameters

TABLE II
DESIGN PARAMETER BOUNDARIES

	a(mm)	b(mm)	c(mm)	d(mm)	e(mm)
Lower boundary	50	50	50	50	50
Upper boundary	500	1000	1000	1000	1200
	f(mm)	g(mm)	h(mm)	x_A(mm)	y_A(mm)
Lower boundary	50	50	50	-400	-400
Upper boundary	1200	1200	1200	400	400
	θ_E(rad)	θ_D(rad)	θ_F(rad)	θ_i(rad)	
Lower boundary	-2π	-2π	-2π	-2π	
Upper boundary	2π	2π	2π	2π	

TABLE III
OPTIMAL DESIGN PARAMETER

	a(mm)	b(mm)	c(mm)	d(mm)	e(mm)
Value (First case)	95	548	366	292	514
Value (Second case)	87	673	545	235	540
	f(mm)	g(mm)	h(mm)	x_A(mm)	y_A(mm)
Value (First case)	419	81	421	55	-239
Value (Second case)	560	84	255	27	-298
	θ_E(rad)	θ_D(rad)	θ_F(rad)	θ_i(rad)	
Value (First case)	2.11	1.8	-1.65	-1.58	
Value (Second case)	2.09	1.69	-1.82	-1.44	

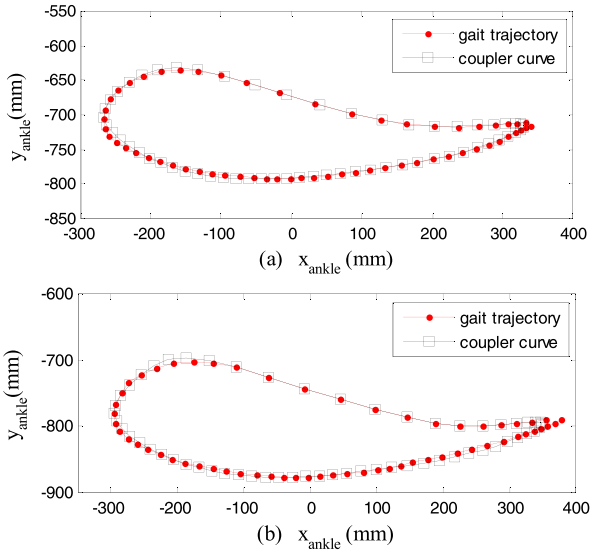

Fig. 7. Gait trajectory and the coupler curve. (a) The height of the subject is 1630 mm. (b) The height of the subject is 1800 mm.

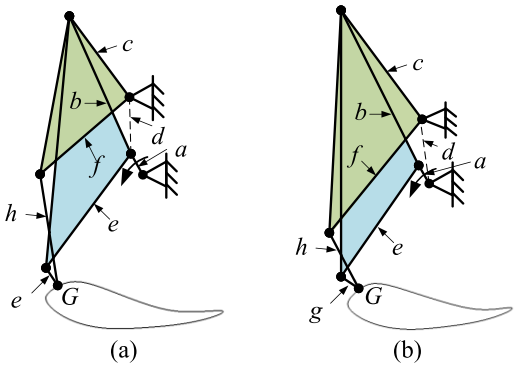

Fig. 8. Sketch of the six-bar linkage mechanism. (a) The height of the subject is 1630mm. (b) The height of the subject is 1800mm.

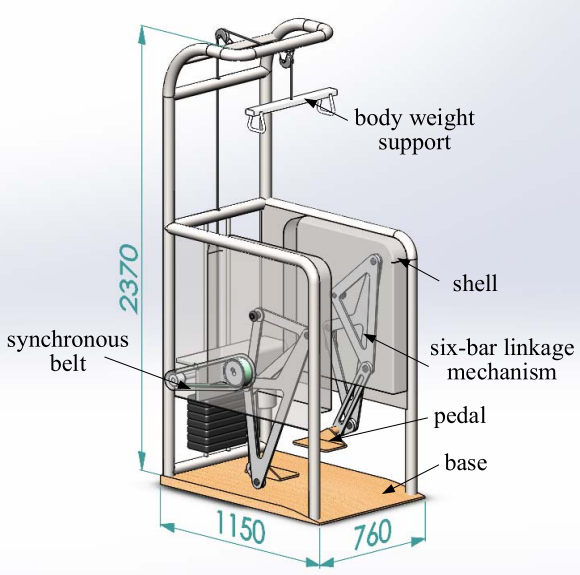

Fig. 9. Three-dimensional model of gait training mechanism in the first case.

TABLE IV
RESULTS OF TWO NUMERICAL IMPLEMENTATIONS

	average distance	maximum distance	sum of distances	Maximum link length	Drive motor
First Case	3.5mm	12mm	225mm	548mm	constant speed
Second Case	5.6mm	15mm	336mm	673mm	constant speed
[37]	11.5mm	--	--	771mm	constant speed

of the six-bar linkage mechanism are shown in Table III. The coupler curve is generated as shown in Fig.7 (b) by driving the crank at a constant speed. From Fig.7 (b), it can be found that the coupler curve matches well with the gait trajectory. The average distance between the 60 precision points is 5.6 mm. The maximum distance is 15 mm, and the sum of distances is 336mm.The final sketch of the six-bar linkage mechanism is shown in Fig.8 (b). The three-dimensional model of gait training mechanism in the first case is shown in Fig.9.

VI. CONCLUSION

In this paper, we propose a new six-bar linkage mechanism for generating natural gait trajectories. Importantly, the design and optimization methods of this mechanism are presented in the mathematic aspect.

The results of two numerical implementations show that the coupler curve matches well with the gait trajectory. As shown in Table IV, in the first case, the average distance between the 60 precision points is 3.5 mm, which is 8 mm less than the cam-linkage mechanism [37]. The maximum distance of the precise point is 12 mm, and the sum of distances is 225 mm. The length of each link is less than 548 mm, which is 223 mm shorter than the cam-linkage mechanism [37]. While, in the second case, the average distance between the 60 precision points is 5.6 mm. Compared with the cam-linkage mechanism [28], the structure is more compact. Furthermore, a constant speed motor is sufficient to control the mechanism and does not need to require a complex cam. By setting the phase difference of the two cranks to 180°, the right and left feet can be guided simultaneously by two identical mechanism controlled by the same motor.

This paper has shown the theoretical possibility of using a six-bar linkage mechanism to simulate the typical foot trajectory in gait for people of different heights, but that both the practicality and clinical relevance of the concept are yet to be demonstrated. In future work, we will build a prototype that can be evaluated first with healthy subjects and then with patients. Furthermore, we will focus on how to simultaneously guide the ankle angle.

REFERENCES

[1] E. L. Miller *et al.*, "Comprehensive overview of nursing and interdisciplinary rehabilitation care of the stroke patient a scientific statement from the American heart association," *Stroke*, vol. 41, no. 10, pp. 2402–2448, Oct. 2010.
[2] J. D. Schaechter, "Motor rehabilitation and brain plasticity after hemiparetic stroke," *Prog. Neurobiol.*, vol. 73, no. 1, pp. 61–72, May 2004.
[3] P. Langhorne, F. Coupar, and A. Pollock, "Motor recovery after stroke: A systematic review," *Lancet Neurol.*, vol. 8, no. 8, pp. 741–754, Aug. 2009.
[4] J. M. Belda-Lois *et al.*, "Rehabilitation of gait after stroke: A review towards a top-down approach," *J. NeuroEng. Rehabil.*, vol. 8, no. 1, pp. 31–42, Dec. 2011, Art. no. 66.
[5] M. Pohl *et al.*, "Repetitive locomotor training and physiotherapy improve walking and basic activities of daily living after stroke: A single-blind, randomized multicentre trial (DEutsche GAngtrainerStudie, DEGAS)," *Clin. Rehabil.*, vol. 21, no. 1, pp. 17–27, Jan. 2007.
[6] J. M. Veerbeek *et al.*, "What is the evidence for physical therapy poststroke? A systematic review and meta-analysis," *PLoS ONE*, vol. 9, no. 2, Feb. 2014, Art. no. e87987.
[7] A. Roy *et al.*, "Robot-aided neurorehabilitation: A novel robot for ankle rehabilitation," *IEEE Trans. Robot.*, vol. 25, no. 3, pp. 569–582, Jun. 2009.
[8] I. Diaz *et al.*, "Lower-limb robotic rehabilitation: Literature review and challenges," *J. Robot.*, vol. 2011, Nov. 2011, Art. no. 759764.
[9] S. Freivogel, J. Mehrholz, T. Husak-Sotomayor, and D. Schmalohr, "Gait training with the newly developed 'LokoHelp'-system is feasible for non-ambulatory patients after stroke, spinal cord and brain injury. A feasibility study," *Brain Injury*, vol. 22, nos. 7–8, pp. 625–632, Jan. 2008.
[10] S. K. Banala, S. K. Agrawal, and J. P. Scholz, "Active leg exoskeleton (ALEX) for gait rehabilitation of motor-impaired patients," in *Proc. IEEE 10th Int. Conf. Rehabil. Robot.*, vol. 1, Jun. 2007, pp. 401–412.
[11] R. Singh, H. Chaudhary, and A. K. Singh, "A novel gait-based synthesis procedure for the design of 4-bar exoskeleton with natural trajectories," *J. Orthopaedic Transl.*, vol. 12, pp. 6–15, Jan. 2018.
[12] J. Yoon *et al.*, "Design of a novel gait rehabilitation robot with upper and lower limbs connections," *J. Inst. Control, Robot. Syst.*, vol. 14, no. 7, pp. 672–678, 2008.

[13] J. Yoon, B. Novandy, C.-H. Yoon, and K.-J. Park, "A 6-DOF gait rehabilitation robot with upper and lower limb connections that allows walking velocity updates on various terrains," *IEEE/ASME Trans. Mechatronics*, vol. 15, no. 2, pp. 201–215, Apr. 2010.

[14] M. Peshkin *et al.*, "KineAssist: A robotic overground gait and balance training device," in *Proc. 9th Int. Conf. Rehabil. Robot. (ICORR)*, 2005, pp. 241–246.

[15] M. Bouri *et al.*, "The WalkTrainer: A robotic system for walking rehabilitation," in *Proc. IEEE Int. Conf. Robot. Biomimetics*, vol. 1, Dec. 2006, pp. 1616–1622.

[16] G. Palestra, M. Rebiai, E. Courtial, and D. Koutsouris, "Evaluation of a rehabilitation system for the elderly in a day care center," *Information*, vol. 10, no. 1, Dec. 2018, Art. no. 3.

[17] M. Bouri, B. Le Gall, and R. Clavel, "A new concept of parallel robot for rehabilitation and fitness: The lambda," in *Proc. IEEE Int. Conf. Robot. Biomimetics (ROBIO)*, Dec. 2009, pp. 2503–2508.

[18] S. Mohan, J. K. Mohanta, S. Kurtenbach, J. Paris, B. Corves, and M. Huesing, "Design, development and control of a 2PRP-2PPR planar parallel manipulator for lower limb rehabilitation therapies," *Mechanism Mach. Theory*, vol. 112, pp. 272–294, Jun. 2017.

[19] M. Girone, G. Burdea, M. Bouzit, V. Popescu, and J. E. Deutsch, "A stewart platform-based system for ankle telerehabilitation," *Auton. Robots*, vol. 10, no. 2, pp. 203–212, Mar. 2001.

[20] J. Nikitczuk, B. Weinberg, P. K. Canavan, and C. Mavroidis, "Active knee rehabilitation orthotic device with variable damping characteristics implemented via an electrorheological fluid," *IEEE/ASME Trans. Mechatronics*, vol. 15, no. 6, pp. 952–960, Dec. 2010.

[21] K. Kora, J. Stinear, and A. McDaid, "Design, analysis, and optimization of an acute stroke gait rehabilitation device," *J. Med. Devices*, vol. 11, no. 1, Mar. 2017.

[22] H. Schmidt, C. Werner, R. Bernhardt, S. Hesse, and J. Krüger, "Gait rehabilitation machines based on programmable footplates," *J. Neuro-Eng. Rehabil.*, vol. 4, no. 1, pp. 1–7, Feb. 2007.

[23] M. F. Bruni, C. Melegari, M. C. De Cola, A. Bramanti, P. Bramanti, and R. S. Calabrò, "What does best evidence tell us about robotic gait rehabilitation in stroke patients: A systematic review and meta-analysis," *J. Clin. Neurosci.*, vol. 48, pp. 11–17, Feb. 2018.

[24] M. Galli, "Robot-assisted gait training versus treadmill training in patients with Parkinson's disease: A kinematic evaluation with gait profile score," *Funct. Neurol.*, vol. 31, no. 3, pp. 163–170, 2016.

[25] S. Hesse, N. Schattat, J. Mehrholz, and C. Werner, "Evidence of end-effector based gait machines in gait rehabilitation after CNS lesion," *NeuroRehabilitation*, vol. 33, no. 1, pp. 77–84, Oct. 2013.

[26] S. Hesse and C. Werner, "Connecting research to the needs of patients and clinicians," *Brain Res. Bull.*, vol. 78, no. 1, pp. 26–34, Jan. 2009.

[27] E. Maranesi *et al.*, "Effectiveness of intervention based on end-effector gait trainer in older patients with stroke: A systematic review," *J. Amer. Med. Directors Assoc.*, vol. 21, no. 8, pp. 1036–1044, Aug. 2020.

[28] P. Sale *et al.*, "Use of the robot assisted gait therapy in rehabilitation of patients with stroke and spinal cord injury," *Eur. J. Phys. Rehabil. Med.*, vol. 48, no. 1, pp. 111–121, 2012.

[29] C. Werner *et al.*, "Treadmill training with partial body weight support and an electromechanical gait trainer for restoration of gait in subacute stroke patients: A randomized crossover study," *Stroke*, vol. 33, pp. 901–2895, Dec. 2002.

[30] P. Alves *et al.*, "Synthesis of a mechanism for human gait rehabilitation: An introductory approach," in *New Trends in Mechanism and Machine Science: From Fundamentals to Industrial Applications*, vol. 24, P. Flores and F. Viadero, Eds. Cham, Switzerland: Springer, 2015, pp. 121–128.

[31] F.-C. Wang, C.-H. Yu, T.-Y. Chou, and N.-C. Chang, "Design and control of an active gait trainer," in *Proc. IEEE Int. Symp. Ind. Electron.*, Jul. 2009, pp. 1762–1770.

[32] B. Y. Tsuge, M. M. Plecnik, and J. Michael McCarthy, "Homotopy directed optimization to design a six-bar linkage for a lower limb with a natural ankle trajectory," *J. Mech. Robot.*, vol. 8, no. 6, pp. 75–81, Dec. 2016.

[33] B. Y. Tsuge and J. M. McCarthy, "Synthesis of a 10-bar linkage to guide the gait cycle of the human leg," in *Proc. 39th Mech. Robot. Conf.*, Aug. 2015, pp. 2015–2021.

[34] R. S. Gonçalves, G. Soares, and J. C. Carvalho, "Conceptual design of a rehabilitation device based on cam-follower and crank-rocker mechanisms hand actioned," *J. Brazilian Soc. Mech. Sci. Eng.*, vol. 41, no. 7, pp. 277–284, Jul. 2019.

[35] Z. Ye and M. R. Smith, "Design of a combined cam-linkage mechanism with an oscillating roller follower by an analytical method," *Proc. Inst. Mech. Eng. C, J. Mech. Eng. Sci.*, vol. 219, no. 4, pp. 419–427, Apr. 2005.

[36] R.-C. Soong, "A new cam-geared mechanism for exact path generation," *J. Adv. Mech. Design, Syst., Manuf.*, vol. 9, no. 2, 2015, Art. no. 1500144.

[37] Y. Shao, Z. Xiang, H. Liu, and L. Li, "Conceptual design and dimensional synthesis of cam-linkage mechanisms for gait rehabilitation," *Mechanism Mach. Theory*, vol. 104, pp. 31–42, Oct. 2016.

[38] L. Yuan and J. S. Rastegar, "Kinematics synthesis of linkage mechanisms with cam integrated joints for controlled harmonic content of the output motion," *J. Mech. Des.*, vol. 126, no. 1, pp. 135–142, Jan. 2004.

[39] D. H. Bhatia *et al.*, "Optimum synthesis of multiloop planar mechanisms for the generation of paths and rigid-body positions by the linear partition of design equations," *J. Eng. Ind.*, vol. 99, no. 1, pp. 855–859, 1976.

[40] H. Mehdigholi and S. Akbarnej, "Optimization of Watt's six-bar linkage to generate straight and parallel leg motion," *Int. J. Adv. Robotic Syst.*, vol. 9, May 2008, Art. no. 22.

[41] L. Mi, M. Guozhi, and L. Qing, "Mathematical modeling and optimization of spiral drum screen in the concrete residue recovery system," *Proc. Inst. Mech. Eng. C, J. Mech. Eng. Sci.*, vol. 234, no. 13, pp. 2624–2630, Jul. 2020.

[42] H. Nollexa, "Linkage coupler curve synthesis: A historical review—III. Spatial synthesis and optimization," *Mechanism Mach. Theory*, vol. 10, no. 1, pp. 41–55, Feb. 1975.

[43] P. Eberhard, "Topology optimization of mechanisms with particle swarm optimization methods," in *Proc. Int. Conf. Mech. Eng. Mech.*, vols. 1–2, 2007, p. 39.

[44] K. Zhang, "Synthesis of a hybrid five-bar mechanism with particle swarm optimization algorithm," in *Proc. Adv. Neural Netw.*, in Lecture Notes in Computer Science, vol. 5263, F. Sun, J. Zhang, Y. Tan, and J. Cao, Eds. Berlin, Germany: Springer, 2008, pp. 873–882.

[45] K. Deb, A. Pratap, S. Agarwal, and T. Meyarivan, "A fast and elitist multiobjective genetic algorithm: NSGA-II," *IEEE Trans. Evol. Comput.*, vol. 6, no. 2, pp. 97–182, Apr. 2002.

[46] V. V. Kovacevic-Vujcic *et al.*, "Stabilization of interior-point methods for linear programming," *Comput. Optim. Appl.*, vol. 14, no. 3, pp. 331–346, 1999.

[47] D. P. Rini, S. M. Shamsuddin, and S. S. Yuhaniz, "Particle swarm optimization: Technique, system and challenges," *Int. J. Comput. Appl.*, vol. 14, no. 1, pp. 19–26, 2011.

[48] D. Tian and Z. Shi, "MPSO: Modified particle swarm optimization and its applications," *Swarm Evol. Comput.*, vol. 41, pp. 49–68, Aug. 2018.

[49] D. Wang, D. Tan, and L. Liu, "Particle swarm optimization algorithm: An overview," *Soft Comput.*, vol. 22, no. 2, pp. 387–408, Jan. 2018.

[50] M. S. Kiran, "Particle swarm optimization with a new update mechanism," *Appl. Soft Comput.*, vol. 60, pp. 670–678, Nov. 2017.

[51] X. Zheng and H. Liu, "A cooperative dual-swarm PSO for dynamic optimization problems," in *Proc. 7th Int. Conf. Natural Comput.*, vol. 2, Jul. 2011, pp. 1131–1135.

[52] Y.-F. Hu, Y.-S. Ding, L.-H. Ren, K.-R. Hao, and H. Han, "An endocrine cooperative particle swarm optimization algorithm for routing recovery problem of wireless sensor networks with multiple mobile sinks," *Inf. Sci.*, vol. 300, pp. 100–113, Apr. 2015.

[53] M. El-Abd, H. Hassan, M. Anis, M. S. Kamel, and M. Elmasry, "Discrete cooperative particle swarm optimization for FPGA placement," *Appl. Soft Comput.*, vol. 10, no. 1, pp. 284–295, Jan. 2010.

[54] M. He, M. Liu, R. Wang, X. Jiang, B. Liu, and H. Zhou, "Particle swarm optimization with damping factor and cooperative mechanism," *Appl. Soft Comput.*, vol. 76, pp. 45–52, Mar. 2019.

[55] H. Ben-Romdhane, S. Krichen, and E. Alba, "A bi-population based scheme for an explicit exploration/exploitation trade-off in dynamic environments," *J. Experim. Theor. Artif. Intell.*, vol. 29, no. 3, pp. 453–479, May 2017.

[56] M. Kapovich *et al.*, "Universality theorems for configuration spaces of planar linkages," *Topology*, vol. 41, no. 6, pp. 1051–1107, Nov. 2002, doi: 10.1016/S0040-9383(01)00034-9.

[57] R. R. Bulatovic *et al.*, "Optimal synthesis of a path generator six-bar linkage," *J. Mech. Sci. Technol.*, vol. 26, no. 12, pp. 4027–4040, Dec. 2012.

[58] U. Onen *et al.*, "Design and actuator selection of a lower extremity exoskeleton," *IEEE/ASME Trans. Mechatronics*, vol. 19, no. 2, pp. 623–632, Apr. 2014.

[59] Y. Shi and R. Eberhart, "A modified particle swarm optimizer," in *Proc. IEEE Int. Conf. Evol. Comput., IEEE World Congr. Comput. Intell.*, New York, NY, USA, May 1998, pp. 69–73.

[60] J. J. Liang, A. K. Qin, P. N. Suganthan, and S. Baskar, "Comprehensive learning particle swarm optimizer for global optimization of multimodal functions," *IEEE Trans. Evol. Comput.*, vol. 10, no. 3, pp. 281–295, Jun. 2006.